JACS
JOURNAL OF THE AMERICAN CHEMICAL SOCIETY

Article

pubs.acs.org/JACS

Electron Transport via Cytochrome C on Si–H Surfaces: Roles of Fe and Heme

Nadav Amdursky,[†,‡] Israel Pecht,[§] Mordechai Sheves,*[,‡] and David Cahen*[,†]

[†]Departments of Materials and Interfaces, [‡]Organic Chemistry, and [§]Immunology, Weizmann Institute of Science, Rehovot 76100, Israel

Supporting Information

ABSTRACT: Monolayers of the redox protein Cytochrome C (CytC) can be electrostatically formed on an H-terminated Si substrate, if the protein- and Si-surface are prepared so as to carry opposite charges. With such monolayers we study electron transport (ETp) via CytC, using a solid-state approach with macroscopic electrodes. We have revealed that currents via holo-CytC are almost 3 orders of magnitude higher than via the heme-depleted protein (→ apo-CytC). This large difference in currents is attributed to loss of the proteins' secondary structure upon heme removal. While removal of only the Fe ion (→ porphyrin-CytC) does not significantly change the currents via this protein at room temperature, the 30–335 K temperature dependence suggests opening of a new ETp pathway, which dominates at high temperatures (>285 K). These results suggest that the cofactor plays a major role in determining the ETp pathway(s) within CytC.

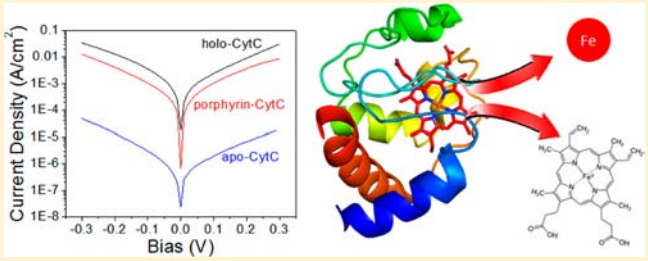

INTRODUCTION

Electron transport (ETp) processes via protein monolayers in the solid state were explored previously in the electron mediator blue Cu protein azurin.[1] In that study it was found that the Cu ion plays an important role in ETp via the protein, which changed from temperature-independent via holo-azurin to a thermally activated process upon Cu ion removal. To explore if this behavior is unique to azurin, we studied ETp via Cytochrome C (CytC), a mitochondrial electron carrier protein that is extensively studied in the quest of understanding electron transfer (ET) reactions.[2,3] ET(p) research within and by CytC has been pursued with a wide variety of methods, including optical spectroscopy,[4,5] electrochemistry,[6,7] and scanning probe microscopy.[8,9]

Here we report results of measuring ETp via monolayers of CytC that has retained only its tightly bound (structural) water and show that removal of either the Fe ion (to yield porphyrin-CytC) or the heme (yielding apo-CytC) markedly affects ETp via the protein. In these solid-state ETp measurements the protein is sandwiched between two electrically conducting and ionically blocking electrodes. Using macroscopic electrodes, one can measure extremely low current densities that are otherwise inaccessible, an option particularly important for measurements at low temperatures. In addition, the macroscopic measurement averages over a large number of molecules ($\sim 10^9$ molecules per junction).[10] This averaging by far surpasses the time averaging as a result of repeated measurements done on a few or even single molecules. Monolayers of the protein are used for macroscopic electrode measurements. We have shown earlier[10] that such monolayers can be prepared, while enabling highly reproducible ETp measurements, by using a very smooth carrier substrate, such as Si. The general approach of using Si is that short (~0.6 nm) linker molecules covalently connect the Si to the protein.[10−12] However, measured currents via the protein (perpendicular to the surface), in a two-terminal configuration, are decreased by the linker and the ~1 nm of regrown SiO_2 layer that are present on the Si surface. These additional layers (linker + SiO_2) can cause orders of magnitude decrease in the current magnitude. Therefore, while measuring the ETp via the protein in a nanoscopic configuration, it is preferable to have it connected directly to an electrode.[8,13−18] Here we show that monolayers of CytC can be formed directly on a freshly etched hydrogen-terminated Si (Si–H) surface, by controlling the Si doping type and the protein's surface charge. We also find that, while the heme removal drastically affects the protein's conformation, removing only the Fe ion has no such effect and also hardly affects the room temperature ETp. However, the role of the Fe in ETp becomes clear from temperature-dependent measurements.

RESULTS AND DISCUSSION

Formation of CytC Monolayers Directly on Si–H Surfaces. Since the isoelectric point of CytC is ~10.0,[19] it is positively charged at neutral pH and negatively only at pH > 10. Therefore, the most common approach to form monolayers of CytC (from a neutral pH solution) is by electrostatic binding to a negatively charged (e.g., carboxylic acid-terminated) linker.[20−22] To explore if a monolayer of CytC can be formed

Received: February 12, 2013
Published: March 21, 2013

   dx.doi.org/10.1021/ja4015474 | J. Am. Chem. Soc. 2013, 135, 6300−6306

by direct electrostatic adsorption to a charged Si surface, we inserted freshly etched (oxide-free) and highly doped n- or p-Si wafers in solutions of 1.5 mg/mL CytC at pH 6 or 11. At these pH values, CytC carries large positive (estimated to be +13)[23] or negative (estimated to be −14)[23] charges, respectively. The secondary structure of CytC, examined by circular dichroism (CD), does not markedly change over this pH range (Figure S1). As shown in Table 1, the thickness, measured by ellipsometry, of the formed CytC layers at pH 6 on p-Si or at pH 11 on n-Si (which from now on will be referred to as "preferred combinations") are significantly larger than those formed by the opposite combinations (CytC at pH 11 on p-Si or at pH 6 on n-Si, to be referred to as the "alternative combinations"). These latter combinations were found to yield thickness values, comparable to those of Si surfaces that were inserted into buffer solutions without the protein at the same pH values. Thus, we interpret these ellipsometry results to mean that with the alternative combinations only an oxide layer is formed on the Si−H surface. We note that also by using the preferred combinations we observe some amount of SiO_x, as will be discussed below.

Table 1. Summary of the Thickness, Contact Angle, Surface Roughness, and Band Banding for the Various Samples

sample	thickness (Å)	contact angle[a] (deg)	surface roughness R.M.S. (Å)	band bending (meV)
n-Si and CytC pH 11	29 ± 2	57 ± 5	7.9 ± 1	53 ± 19
n-Si and CytC pH 6	19 ± 1	25	3.6 ± 0.6	171 ± 10
p-Si and CytC pH 11	17 ± 1.5	22	3.4 ± 0.5	165 ± 11
p-Si and CytC pH 6	31 ± 2.5	52 ± 5	8.1 ± 1	52 ± 18
n-Si and buffer pH 11	15 ± 1	20	2.5 ± 0.3	201 ± 10
n-Si and buffer pH 6	16 ± 1	19	2.6 ± 0.3	200 ± 7
p-Si and buffer pH 11	14 ± 1.5	19	2.7 ± 0.3	195 ± 15
p-Si and buffer pH 6	15 ± 1.5	18	2.8 ± 0.3	199 ± 20

[a]Contact angle measurements on very hydrophilic surfaces are inaccurate, and values below 25° are estimated ones.

To further characterize the surfaces, produced by the preferred combinations, we measured their surface morphology by atomic force microscopy (AFM) (Table 1 and Figure 1a−d) and their water contact angle (Table 1 and Figure 1e−h). As seen in the AFM images, the preferred combinations yield relatively rough surfaces (Figure 1a and b), which are consistent with the presence of a protein monolayer, as we have observed in previous studies.[10] The AFM images of surfaces, produced by the alternative combinations (Figure 1c and d), show relatively smooth surfaces, consistent with SiO_x. Surfaces of SiO_x are known to be highly hydrophilic, as seen in the control experiments (Table 1), similar to those obtained using the alternative combinations (Figure 1g and h). The surfaces prepared by the preferred combinations exhibit a larger contact angle (~55°, Figure 1e and f), most probably due to the significant number of Lys residues on the protein surface, consistent with an amine-terminated Si surface.[24] In an additional important control experiment, we inserted a Si wafer, already covered with a thin oxide layer (~15 Å), into protein solutions, using the preferred combinations. In this case we did not observe any surface thickness increase, nor a change in the surface morphology (Figure S2), consistent with the lack of protein adsorption. This supports the direct adsorption of CytC on the Si−H surface only when the preferred combinations are employed.

To quantitate the ratio of formed SiO_x to that of adsorbed protein molecules, we used X-ray photoelectron spectroscopy (XPS) of the surfaces, produced by the preferred combinations. Table 2 presents the stoichiometric ratios of C to N, O, and $Si(O_x)$ (the Si 2p XPS peak at ~103 eV is assigned to SiO_x and not to bulk Si). The XPS results confirm both the presence of the protein on the surface and provide an estimate of the relatively small amount of SiO_x in comparison to the C atoms of CytC. The presence of a protein layer on the surfaces was also confirmed by measuring the Fourier transform infrared

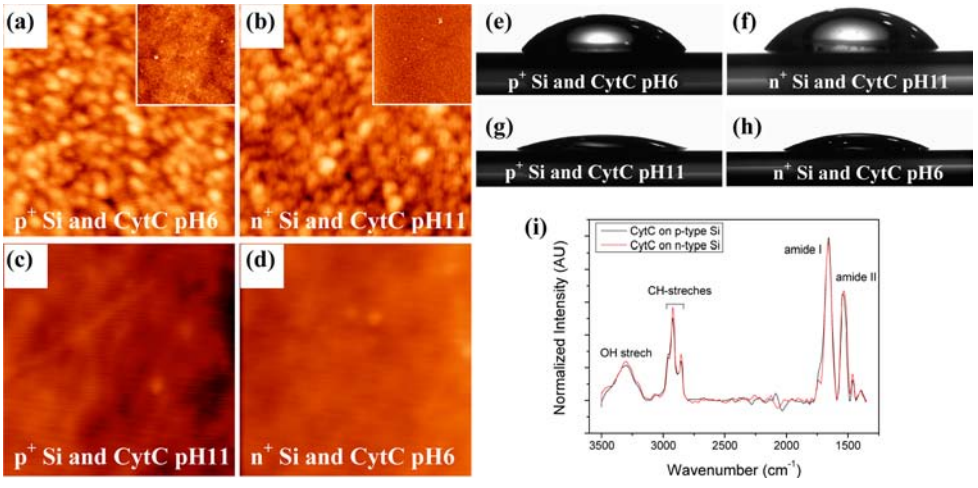

Figure 1. Si surfaces covered with CytC. (a−d) AFM morphology of the surfaces at the preferred (a and b) and the alternative (c and d) combinations. The dimensions of the squares are 500 × 500 nm; the *Z* scale is 6 nm. The insets in a and b are lower magnifications of the surfaces with dimensions of 3 × 3 μm. (e−h) The contact angle of a drop of water on top of the surfaces at the preferred (e and f) and the alternative (g and h) combinations. (i) FT-IR spectrum of Si surfaces, covered with CytC for the preferred combinations.

dx.doi.org/10.1021/ja4015474 | J. Am. Chem. Soc. 2013, 135, 6300−6306

Table 2. XPS Element Ratios

	C:N	C:O	C:Si(O_x)
theoretical ratios for CytC	3.8	3.6	
n-Si and CytC pH 11	4.0	2.8[a]	6.9
p-Si and CytC pH 6	4.0	2.9[a]	8.3

[a]The lower values of C:O are probably due to bound water molecules of the CytC molecules.

(FT-IR) spectra (measured by Ge-attenuated total reflectance, G-ATR) of the surfaces, prepared by the preferred combinations (Figure 1i), which show the amide I/II stretches.

The adsorption of CytC on Si using the preferred combinations changes the electronic properties of the Si surface. The depletion layer of n- or p-Si has a positive or negative charge, respectively. These charges are neutralized by opposite charges on/near the surface; that is, the depletion layer charge implies that the surface states of n-Si are negatively charged, and those of p-Si are positively charged. The larger the charge density of the surface states, the stronger is their band bending (BB). H-terminated Si surface is very well passivated electronically; i.e., the density of charged surface states is very low, corresponding to a small BB (~40 meV). Insertion of the H-terminated Si wafers into the aqueous buffer caused an increase in the BB to ~200 meV (Table 1). Increases in BB were also observed for the surfaces prepared from the nonpreferred Si-CytC combinations. However, the Si-CytC surfaces that were produced by the preferred combinations yielded only a very small increase (10 meV) in BB (Table 1). Such small increase in BB can be rationalized as follows: adsorption of positively charged CytC (at pH 6) onto p-Si (and vice versa for negatively charged CytC on n-Si) blocks the surface with the protein and, thus, minimizes the uncontrolled growth of an oxide layer (with uncontrolled charges in it) that occurs if the surface is exposed (for ~20 min) to the buffer solution.

Comparison of ETp via CytC on Si–H with That via Proteins on Linkers. The current densities via the monolayers were measured with Hg as one contact and a highly doped, nearly degenerate, Si substrate as the other, in a two-electrode configuration. As seen in Figure 2a, the measured currents via the CytC monolayers for the two preferred combinations are very similar, thus confirming the similarity between the formed protein monolayers. Moreover, the current density magnitude via the CytC layer is orders of magnitude lower than that via the thin SiO_x layer that formed when the Si–H surface was inserted into the buffer solution without the protein. This is consistent with the measured ETp occurring via the protein. As mentioned above, the formation of a protein layer directly on Si surface should significantly increase the measured current magnitude via the protein, compared to protein monolayers attached via linkers. Figure 2b shows the room temperature current densities via the CytC monolayer on p-Si–H in comparison to those via monolayers of CytC, azurin, or bacteriorhodopsin, formed by using propyl-silane linkers (see the schematic in Figure 2b).[10] Indeed, the current densities via the CytC monolayer, electrostatically adsorbed directly on the Si–H surface, is ~2.5 orders of magnitude larger than via proteins that were connected by propyl-silane linker molecules on SiO_x.[25] These 2.5 orders of magnitude correspond well to the decrease in current that is expected for the transport across the additional ~7 Å of linker (by using a distance decay constant of β = 0.8–0.9 $Å^{-1}$ for saturated molecules). As

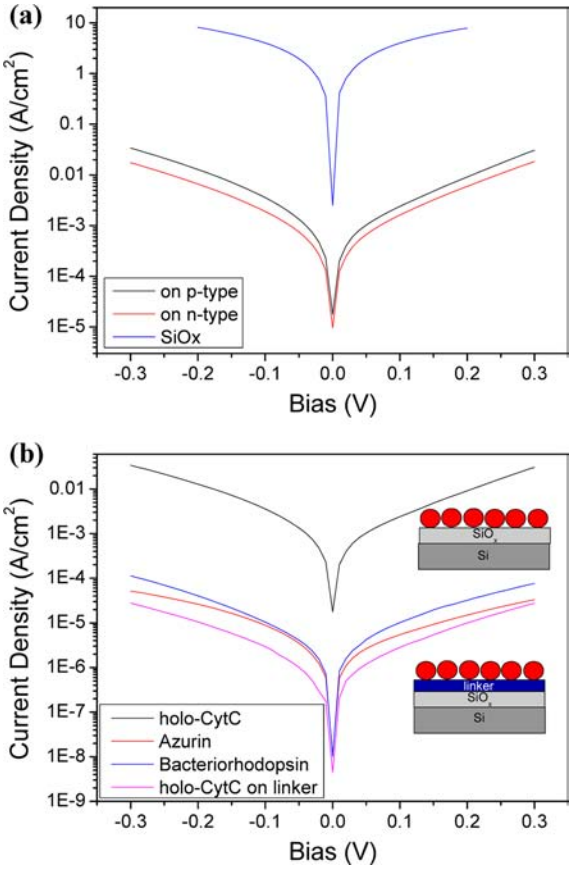

Figure 2. Current density–voltage plots for Hg/protein monolayer/substrate systems with different proteins and substrates. (a) CytC monolayers on p- and n-Si, and a reference sample with ~15 Å SiO_x only; (b) CytC monolayers, directly on Si–H and monolayers of CytC, azurin, and bacteriorhodopsin, formed by using propyl-silane linker monolayers on ~10 Å regrown SiO_x.

indicated by results of the XPS (Table 2), and similar to systems where proteins are linked to propyl-silane linkers, these CytC surfaces also contain some SiO_x. Results of measurements of the conductivity and capacitance of SiO_x as a function of the SiO_x thickness in the range of 1–2 nm show little current reduction between 1 and 2 nm of oxide. This leads to the conclusion that there is significant current leakage through the oxide layer, which can be explained by the nonstoichiometry of, and defect density in such thin films (see further discussion and figures in the Supporting Information).[26,27] Thus, while the absence of the organic linker layer is very important here, in that it increases the observed currents, the thinner oxide film in our present configuration, compared to the previous one,[1,10] has no significant effect.

ETp via Holo-, Porphyrin-, and Apo-CytC. To explore the factors that influence ETp via CytC, we compared ETp via holo-CytC with Fe-free (porphyrin-CytC), and with heme-depleted (apo-CytC) derivatives. We have used holo-CytC to prepare both porphyrin-CytC and apo-CytC in solution (see Materials and Methods section). The successful preparation of the proteins' derivatives was confirmed by UV–vis absorption and CD spectroscopies (Figure 3a and b, respectively). The UV–vis absorption (Figure 3a) shows the strong typical porphyrin Soret band (~400 nm) of holo- and porphyrin-CytC, while apo-CytC lacks this band. Further support for the formation of porphyrin-CytC is derived from the different

dx.doi.org/10.1021/ja4015474 | J. Am. Chem. Soc. 2013, 135, 6300–6306

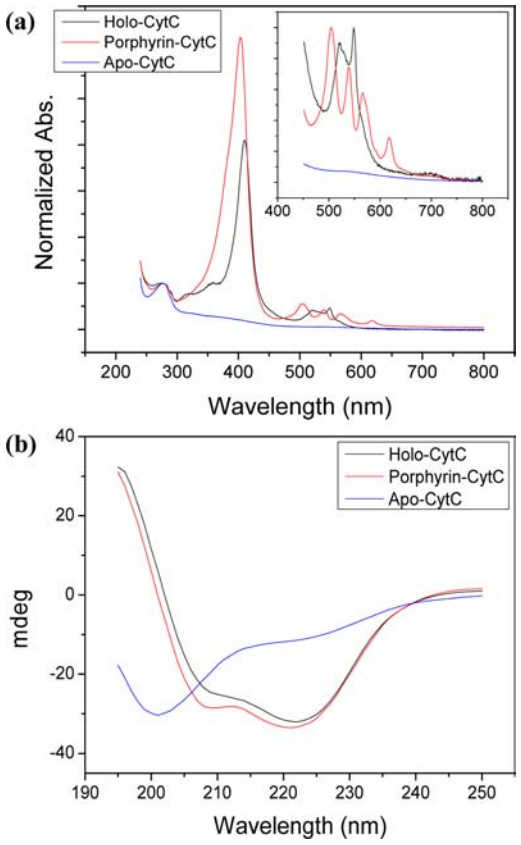

Figure 3. (a) UV−vis and (b) CD absorption spectroscopy of holo- (black curve), porphyrin- (red curve), and apo-CytC (blue curve) solutions. The inset of a shows a zoom-in on the longer wavelength range.

charge transfer band of the heme group at the longer wavelength part of the spectrum in comparison to holo-CytC (inset of Figure 3a), which corresponds to that observed in earlier studies of porphyrin-CytC.[28] The CD spectra (Figure 3b) show that removal of the Fe ion did not change the secondary structure of the protein, while removal of the heme group significantly changed the structure to a random coil structure, which has previously been assigned to the unfolded state of holo-CytC.[29]

The room temperature current density via the three CytC forms (Figure 4a) shows that, while the current magnitude via porphyrin-CytC is comparable to that of holo-CytC (∼2 times smaller), the current magnitude via apo-CytC is almost 3 orders of magnitude smaller. The smaller current magnitude via apo-CytC indicates the importance of the heme or porphyrin group and, probably more importantly, of the protein's native conformation for ETp. Sharp decreases in the current magnitudes were previously observed for several types of proteins and peptides upon either thermally induced denaturation,[1,30] or unfolding the helical structure of peptides by changing the pH,[31] as well as by physically stretching the peptide.[32] These observations support our interpretation that the ETp is primarily determined by the proteins' conformation.

To further explore the ETp mechanism via the CytC derivatives we measured the current density as a function of temperature. Figure 4b shows the current density at a low bias (50 mV) as a function of $1000/T$. The ETp via the CytC surfaces (of the three derivatives) exhibits two regimes, a temperature-independent one at low temperatures (≤185, 195, and 170 K for holo- porphyrin- and apo-CytC, respectively), and a thermally activated one, at higher temperatures. At the same time, for a sample without protein high temperature-independent currents over the whole temperature range were measured. The temperature-independent process of the latter is consistent with electron tunneling through a thin (14−16 Å) layer of SiO_x. Tunneling is, to a first approximation, a temperature-independent process, in which the current is proportional to: $\exp(-\beta l)$, with β = the distance-decay constant and l = the separation distance over which tunneling occurs, which, here, is the geometrical separation between the electrodes. Thus, temperature-independent ETp at low temperatures via proteins (which characterizes all proteins that we have studied so far)[1,30,33,34] is consistent with electron tunneling. Because the distance between the electrodes, l, determined by the protein height (∼30−33 Å), is larger than the distance in the control experiment where only SiO_x was present, it is reasonable that the amplitudes of tunneling currents via the proteins are much lower than via SiO_x. Similar to the current magnitude at room temperature (Figure 4a), also in the low temperature regime there is a large difference between the ETp via holo-/porphyrin-CytC to that via apo-CytC. Though the widths of the layers are comparable, and in fact that of apo-CytC was statistically lower (by ∼3 Å) than of the other two derivatives (probably due to the loss of the secondary structure), currents via apo-CytC are 40 and 70 times lower than those through porphyrin- and holo-CytC, respectively. This difference suggests that both the heme and porphyrin provide energy levels which facilitate tunneling ("Superexchange"). Alternatively, or in addition, the presence of the relatively exposed heme or porphyrin may increase coupling to one of the electrodes.

The temperature-dependent change in current density in the high-temperature regime can be fitted to an Arrhenius equation, with current $\alpha \exp(-E_a/k_BT)$, yielding the thermal activation energy, E_a (Figure 4c). As seen in the figure, while the ETp via holo-CytC fits to a single activation energy value (E_a = 105 meV), the ETp via porphyrin-CytC has two activation energies of 105 (at 200−285 K) and 550 meV (in the 285−335 K range). According to Marcus theory,[35] a thermally activated ET process originates from the vibrational modes of the ET pathway. This dependence can be observed if the thermal energy is larger than half of the vibrational mode energy, $2k_BT > \hbar\omega$. The identical value of activation energy calculated from the data in the thermally activated regime for holo-CytC and porphyrin-CytC over the 200−285 K range, suggests that a similar ETp pathway operates in these two CytC forms over this temperature regime. The conformational similarity between holo- and porphyrin-CytC (Figure 3b) suggests that the ETp pathway with E_a = 105 meV can be ascribed to vibrational modes that are associated with the proteins' structure.

The high activation energy regime of porphyrin-CytC suggests an additional ETp pathway, associated with higher energy vibrational modes, which is operative only upon removal of the Fe ion. In accordance to Kirchhoff's law, current flows via the pathway of least resistance. Thus, the high E_a pathway can be observed only at high temperatures, where its transport is higher than via the low E_a pathway. A similar pattern has previously been observed in the ETp via bacteriorhodopsin (bR),[30] where the calculated E_a depended on whether the retinal (the cofactor of bR) was covalently bound to the protein or not, while two E_a regimes were observed for the ETp via

dx.doi.org/10.1021/ja4015474 | J. Am. Chem. Soc. 2013, 135, 6300−6306

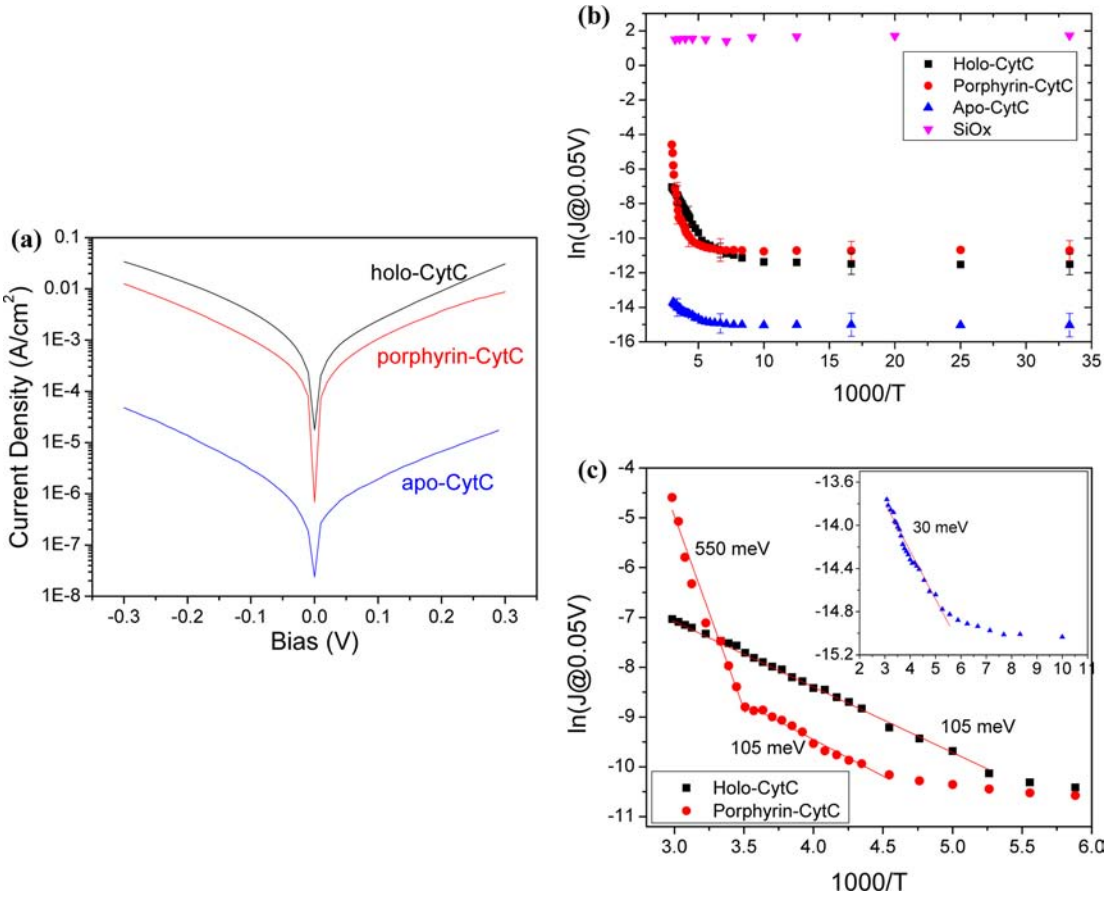

Figure 4. ETp via CytC derivatives. (a) Room-temperature J–V and (b) temperature-dependent J @ 0.05 V as function of 1000/T via holo-, porphyrin-, and apo-CytC and of ~1.5 nm SiO_x. (c) Arrhenius plots of the data in the thermally activated regime, along with the calculated thermal activation energies. The inset shows a zoom-in on the high temperature data for apo-CytC.

reconstituted-bR. Also, we have observed that retinoate can induce marked conductivity to albumin.[34] All these results are in line with the current findings that conjugated small molecules, as the porphyrin in CytC, can be major contributors to the ETp via a protein. The role of Fe in the ETp process via CytC is another example of the importance of a metal ion for electron transport.[1] In azurin, removal of the Cu ion, which does not affect the protein's structure, changed a temperature-independent ETp to a thermally activated process at T > 200 K, with a 320 meV activation barrier.[1] The very low E_a of apo-CytC (inset of Figure 4c) indicates that a distinct ETp pathway is operative, different from that in porphyrin-/holo-CytC. Moreover, as mentioned above, it underscores the importance of the protein conformation, also in solid state ETp.

Macroscopic Solid-State ETp via Protein Monolayers on Si–H. Results of this study have several major implications. The first relates to the more fundamental understanding of ET(p) via proteins. The main experimental methods employed in monitoring ET via proteins are spectroscopy,[36,37] electrochemistry,[38−40] nanoscale surface methods (scanning tunneling or atomic force microscopies),[17,41,42] and macroscopic scale electrical transport.[1,10,30] The first two methods are mainly employed in solution and require the presence of an electron donor/acceptor within the protein or its modification by incorporating a donor and/or acceptor. The latter two approaches can be performed in the solid state to measure the ETp across the protein, without requiring an internal electron donor/acceptor. Nanoscale methods allow studies of a few (or even single) molecule(s) but have low sensitivity and high variability (necessitating time-averaging, i.e., many sequential measurements). Also, in most cases, the tip force that has to be applied to perform the electrical measurements will influence the results, and more seriously,[43] this force may vary significantly during measurement, such as those with retracting STM tip. With the nanoscale, as well as the first two methods, temperature-dependence measurements over a wide range are problematic. Macroscopically one can measure orders of magnitude lower current densities than those monitored by nanoscale methods. As we have observed here, the protein's native conformation has a crucial role in the current density via the protein. Hence, the low currents (at low biases) via apo-CytC cannot be measured by nanoscale electrodes, and using macroscopic electrodes may be the only way to resolve and compare the ETp across folded and unfolded proteins. Quantitatively, the nanoscale-based approaches for measuring the ETp via WT CytC resulted in measured current densities (at 0.1 V, and, for AFM, at >10 nN tip force) of 4×10^{-12} and 1×10^{-11} A/nm^2 in atomic force[8] and scanning tunneling[9] microscopy configurations, respectively, using the reported contact areas. However, these current densities are close to the detection limits of the instrumental configuration, using a conventional nanoscale tip. Because we observed here that the currents via apo-CytC are almost 3 orders of magnitude lower than via holo-CytC, detecting the current via apo-CytC by the nanoscale approaches (at low bias and low force) is apparently not feasible. Generally, the measured current densities by the

dx.doi.org/10.1021/ja4015474 | J. Am. Chem. Soc. 2013, 135, 6300−6306

macroscopic approaches are several orders of magnitude lower than by the nanoscale ones (for an extensive review see ref 44). Indeed, the current densities measured in this work for holo- and apo-CytC are 2.5×10^{-17} and 2×10^{-20} A/nm^2, respectively, which, for holo-CytC is more than 5 orders of magnitude lower than that measured by the nanoscale approaches. Thus, for apo-CytC it is only thanks to the 9−10 orders of magnitude larger contact areas than with conventional tips employed by nanoscale approaches, that the ETp measurements via the monolayer can give signals with useful S/N.

The second implication is of a more applied nature and is related to the use of (initially oxide-free) Si as a template for biosensors or bioelectronic components. During the last years great progress was made in using Si electrodes, mainly Si nanowires, for biosensing.[45,46] The ability to functionalize the surface of freshly etched Si with proteins, without the need for additional intermediate layers between the protein and Si, can increase the electrical sensitivity of the electrode and may well be important for future bioelectronic devices.

CONCLUSIONS

We succeeded in forming monolayers of different CytC derivatives on freshly etched Si−H surfaces by employing the protein's intrinsic charges (determined by the pH of the solution) and those of the Si surface charge (determined by the Si doping). We confirmed the layer formation of a positively charged protein (at pH 6) on p-Si and a negatively charged protein (at pH 11) on n-Si. Monitoring ETp via such CytC monolayers as a function of temperature (30−335 K), we could explore the role of the Fe ion and the porphyrin ring in the ETp process. We observed that maintaining the protein's native folding (which depends on the presence of the porphyrin ring) is crucial for the ETp. The thermally activated ETp pathway via holo-CytC appears to be also operative in porphyrin-CytC, but the latter form of the protein has an additional ETp pathway, which dominates at high temperatures. The apo-CytC, which is unfolded, shows ETp efficiency, which is orders of magnitude lower than via porphyrin- and holo-CytC, and does not exhibit any of these ETp pathways. The low ETp via apo-CytC can, probably, only be observed with macroscopic-scale electrodes as done here, while the absence of porphyrin markedly affects electrochemical or spectroscopic measurements of ET.

MATERIALS AND METHODS

Porphyrin- and Apo-CytC Preparation. Wild type horse heart CytC (Sigma-Aldrich) was used for the preparation of both porphyrin- and apo-CytC. We followed the protocol of Vanderkooi and Erecinska[28] for the preparation of porphyrin-CytC with minor modifications. A sample of 50 mg of CytC was cooled in a plastic beaker suspended in a Dewar flask containing acetone and dry ice. About 6 mL of anhydrous HF was passed into the plastic beaker, while continuous stirring the solution with a Teflon rod for 5 min (the CytC turned purple during the process). The plastic beaker was transferred from the cold acetone to room temperature, and the HF was removed with a stream of nitrogen. The protein pellet was dissolved in 3 mL of 0.05 M ammonium acetate, pH 5. The protein was eluted with a Sephadex G-50 column by using 0.05 M ammonium acetate, pH 5. We used the protocol of Fisher et al.[47] (without modifications) for the preparation of apo-CytC. The protein fractions of both porphyrin- and apo-CytC were divided into two, and the buffer was replaced to 10 mM phosphate buffer, pH 6 or 11, by using an Amicon Centricon (4 KDa cutoff).

UV−vis Absorption Measurements. The UV−vis absorption measurements were taken with a Cary 5000 UV−vis-NIR spectrophotometer, using a 10 mm quartz cuvette. A 10 mM phosphate buffer was used as a baseline.

Circular Dichroism (CD) Measurements. The CD spectra were measured on a Chirascan spectrometer. The solution measurements were made using a 1 mm optical-path quartz cuvette. A 10 mM phosphate buffer was used as a baseline.

Surface Preparation. Highly doped p- (<0.001 Ω cm) or n- (0.001−0.005 Ω cm) type Si surfaces ⟨100⟩ were used. The Si surfaces were cleaned by bath sonication in ethyl acetate/acetone/ethanol (2 min in each) and were thoroughly rinsed in Milli-Q (18 MΩ) water. Then the surface undergone two cycles of 30 min of piranha treatment (7/3 v/v of H_2SO_4/H_2O_2) at 80 °C (***Caution**: piranha solutions are extremely corrosive, reactive, and potentially explosive*) and 90 s in 2% HF solution (the surfaces were thoroughly rinsed in Milli-Q water between the piranha treatment and the insertion to the 2% HF solution). At the end of the second cycle, the surfaces were quickly rinsed in water and immersed in a sealed vial containing 10 mM phosphate buffer solution, at pH 6 or pH 11, with or without the protein (0.1 mM), for 30 min, followed by cleaning the surfaces with Milli-Q water and drying them with a gentle N_2 stream.

Ellipsometry Measurements. The ellipsometry measurements were performed with a Woollam M-2000 V multiple-wavelength ellipsometer at an angle of incidence of 70°. The Cauchy model was used to estimate the thickness of the organic layers, and the SiO_2 model was used to estimate the thickness of the oxide layer in the control experiments. There were no substantial differences between the results, obtained with the two models.

Contact Angle Measurements. Static contact angle measurements were performed with an automated goniometer (Ramé-Hart, model-100). Approximately 4 μL of deionized water (Millipore Inc.) was deposited onto the sample, using a microsyringe (advancing drop method). Measurements were recorded immediately after deposition.

AFM Imaging. The topography of the surfaces was characterized by AFM in a semicontact mode. A Solver P47 SPM system (NT-MDT, Zelenograd Russia) and Si probes (NSC36, 75kHz, 0.6 N/m, MIKROMASCH) were used.

Contact Potential Difference (CPD). CPD measurements were conducted with a home-built apparatus to measure the work function, based on a commercial Besocke Delta Phi Kelvin probe. The band bending was estimated by measuring the difference between the CPD with the sample in the dark and under strong illumination (~0.5 W/cm^2). The measurements were done inside a Faraday cage, in order to minimize electrical noise.

Ge-Attenuated Total Reflectance (G-ATR) Fourier Transform Infrared (FT-IR) Spectroscopy. G-ATR FT-IR measurements were conducted with a Nicolet 6700 spectrometer with a liquid-N2-cooled (Hg,Cd)Te detector, while the sample was pressed onto a Ge crystal. The spectra were corrected for background by subtracting a reference spectrum obtained from a freshly cleaned and etched Si sample.

X-ray Photoelectron Spectroscopy (XPS). XPS measurements were carried out with a Kratos AXIS ULTRA system, using a monochromatic Al ($K\alpha$) X-ray source ($h\nu$ = 1486.6 eV) at 75 W and detection pass energies between 10 and 80 eV, with a takeoff angle of 65°.

Current−Voltage Measurements. The top contact was made by placing a drop of Hg (~500 μm in diameter) by capillary on top of the protein monolayer. InGa was used as a back contact by scratching the back side of the Si surface and rubbing an eutectic paste of InGa onto it. Using a macroscopic contact area results in instant spatial averaging of the ETp via 10^9−10^{10} proteins,[10] so that the measurement error of the currents is low, even for electrostatically nonspecifically bound proteins (as we also showed previously for serum albumins[1,10,34]). For temperature-controlled measurements, the sample was placed in a vacuum chamber in a TTPX cryogenic four-probe electrical measurement system (Lakeshore), and both the sample holder and the probes were cooled. The temperature was monitored and controlled with an accuracy of 0.2 K. To allow the sample to reach thermal equilibrium, the sample was not measured *between* each change in temperature.

dx.doi.org/10.1021/ja4015474 | J. Am. Chem. Soc. 2013, 135, 6300−6306

■ ASSOCIATED CONTENT

Supporting Information

CD spectra, AFM image, and supplemental discussion and figures about conductance and capacitance via oxide layers. This material is available free of charge via the Internet at http://pubs.acs.org.

■ AUTHOR INFORMATION

Corresponding Author

David.Cahen@weizmann.ac.il; mudi.sheves@weizmann.ac.il

Notes

The authors declare no competing financial interest.

■ ACKNOWLEDGMENTS

We are deeply indebted to Prof. Y. Shai for his help in preparation of Fe free CytC, to Y. Barak for assisting with the liquid chromatography purification, and S. Raichlin for the production of apo-CytC. We further thank DC group members and E. Moons (Karlstad Univ., Sweden) for fruitful discussions. N.A. thanks the Clore Foundation Fellowship, and M.S. thanks the Kimmelman center for Biomolecular Structure and Assembly for its support. We thank the Minerva Foundation (Munich) for partial support. M.S. holds the Katzir-Makineni chair in Chemistry. D.C. holds the Schaefer Chair in Energy Research.

■ REFERENCES

(1) Sepunaru, L.; Pecht, I.; Sheves, M.; Cahen, D. *J. Am. Chem. Soc.* **2011**, *133*, 2421.
(2) Ferguson-Miller, S.; Brautigan, D. L.; Margoliash, E. *J. Biol. Chem.* **1976**, *251*, 1104.
(3) Pelletier, H.; Kraut, J. *Science* **1992**, *258*, 1748.
(4) Nocera, D. G.; Winkler, J. R.; Yocom, K. M.; Bordignon, E.; Gray, H. B. *J. Am. Chem. Soc.* **1984**, *106*, 5145.
(5) Gray, H. B.; Winkler, J. R. *Biochim. Biophys. Acta-Bioenerg.* **2010**, *1797*, 1563.
(6) Tarlov, M. J.; Bowden, E. F. *J. Am. Chem. Soc.* **1991**, *113*, 1847.
(7) Bortolotti, C. A.; Borsari, M.; Sola, M.; Chertkova, R.; Dolgikh, D.; Kotlyar, A.; Facci, P. *J. Phys. Chem. C* **2007**, *111*, 12100.
(8) Davis, J. J.; Peters, B.; Xi, W. *J. Phys.: Condens. Matter* **2008**, *20*, 374123.
(9) Khomutov, G. B.; Belovolova, L. V.; Gubin, S. P.; Khanin, V. V.; Obydenov, A. Y.; Sergeev-Cherenkov, A. N.; Soldatov, E. S.; Trifonov, A. S. *Bioelectrochemistry* **2002**, *55*, 177.
(10) Ron, I.; Sepunaru, L.; Itzhakov, S.; Belenkova, T.; Friedman, N.; Pecht, I.; Sheves, M.; Cahen, D. *J. Am. Chem. Soc.* **2010**, *132*, 4131.
(11) Amador, S. M.; Pachence, J. M.; Fischetti, R.; McCauley, J. P.; Smith, A. B.; Blasie, J. K. *Langmuir* **1993**, *9*, 812.
(12) Maruccio, G.; Biasco, A.; Visconti, P.; Bramanti, A.; Pompa, P. P.; Calabi, F.; Cingolani, R.; Rinaldi, R.; Corni, S.; Di Felice, R.; Molinari, E.; Verbeet, M. P.; Canters, G. W. *Adv. Mater.* **2005**, *17*, 816.
(13) Xu, D.; Watt, G. D.; Harb, J. N.; Davis, R. C. *Nano Lett.* **2005**, *5*, 571.
(14) Della Pia, E. A.; Elliott, M.; Jones, D. D.; Macdonald, J. E. *ACS Nano* **2012**, *6*, 355.
(15) Frascerra, V.; Calabi, F.; Maruccio, G.; Pornpa, P. P.; Cingolani, R.; Rinaldi, R. *IEEE Trans. Nanotechnol.* **2005**, *4*, 637.
(16) Inkpen, M. S.; Albrecht, T. *ACS Nano* **2012**, *6*, 13.
(17) Zhao, J. W.; Davis, J. J.; Sansom, M. S. P.; Hung, A. *J. Am. Chem. Soc.* **2004**, *126*, 5601.
(18) Rakshit, T.; Banerjee, S.; Mukhopadhyay, R. *Langmuir* **2010**, *26*, 16005.
(19) Lvov, Y.; Ariga, K.; Ichinose, I.; Kunitake, T. *J. Am. Chem. Soc.* **1995**, *117*, 6117.
(20) Lee, J. B.; Kim, D. J.; Choi, J. W.; Koo, K. K. *Mater. Sci. Eng., C* **2004**, *24*, 79.
(21) Ataka, K.; Heberle, J. *J. Am. Chem. Soc.* **2004**, *126*, 9445.
(22) Avila, A.; Gregory, B. W.; Niki, K.; Cotton, T. M. *J. Phys. Chem. B* **2000**, *104*, 2759.
(23) Putnam, C. In http://www.scripps.edu/~cdputnam/protcalc.html; The Scripps Research Institute: La Jolla, CA, 2006.
(24) Hong, H. G.; Jiang, M.; Sligar, S. G.; Bohn, P. W. *Langmuir* **1994**, *10*, 153.
(25) The thickness, measured by ellipsometry, of CytC on p-Si-H is ~30 Å, while the thickness of CytC on a Si−SiO_x-linker is ~35 Å.
(26) Buchanan, D. A.; Stathis, J. H.; Cartier, E.; DiMaria, D. J. *Microelectron. Eng.* **1997**, *36*, 329.
(27) Rodriguez, R.; Miranda, E.; Pau, R.; Sune, J.; Nafria, M.; Aymerich, X. *Microelectron. Reliab.* **2000**, *40*, 707.
(28) Vanderkooi, J. M.; Erecinska, M. *Eur. J. Biochem.* **1975**, *60*, 199.
(29) Stellwagen, E.; Rysavy, R.; Babul, G. *J. Biol. Chem.* **1972**, *247*, 8074.
(30) Sepunaru, L.; Friedman, N.; Pecht, I.; Sheves, M.; Cahen, D. *J. Am. Chem. Soc.* **2012**, *134*, 4169.
(31) Scullion, L.; Doneux, T.; Bouffier, L.; Fernig, D. G.; Higgins, S. J.; Bethell, D.; Nichols, R. J. *J. Phys. Chem. C* **2011**, *115*, 8361.
(32) Lopez-Perez, D. E.; Revilla-Lopez, G.; Jacquemin, D.; Zanuy, D.; Palys, B.; Sek, S.; Aleman, C. *Phys. Chem. Chem. Phys.* **2012**, *14*, 10332.
(33) Amdursky, N.; Pecht, I.; Sheves, M.; Cahen, D. *Proc. Natl. Acad. Sci.* **2013**, *110*, 507.
(34) Amdursky, N.; Pecht, I.; Sheves, M.; Cahen, D. *J. Am. Chem. Soc.* **2012**, *134*, 18221.
(35) Marcus, R. A.; Sutin, N. *Biochim. Biophys. Acta* **1985**, *811*, 265.
(36) Gray, H. B.; Winkler, J. R. *Q. Rev. Biophys.* **2003**, *36*, 341.
(37) Farver, O.; Pecht, I. *Coord. Chem. Rev.* **2011**, *255*, 757.
(38) Murgida, D. H.; Hildebrandt, P. *Phys. Chem. Chem. Phys.* **2005**, *7*, 3773.
(39) Udit, A. K.; Gray, H. B. *Biochem. Biophys. Res. Commun.* **2005**, *338*, 470.
(40) Andolfi, L.; Bruce, D.; Cannistraro, S.; Canters, G. W.; Davis, J. J.; Hill, H. A. O.; Crozier, J.; Verbeet, M. P.; Wrathmell, C. L.; Astier, Y. *J. Electroanal. Chem.* **2004**, *565*, 21.
(41) Friis, E. P.; Andersen, J. E. T.; Madsen, L. L.; Moller, P.; Ulstrup, J. *J. Electroanal. Chem.* **1997**, *431*, 35.
(42) Tao, N. J. *Phys. Rev. Lett.* **1996**, *76*, 4066.
(43) Li, W.; Sepunaru, L.; Amdursky, N.; Cohen, S. R.; Pecht, I.; Sheves, M.; Cahen, D. *ACS Nano* **2012**, *6*, 10816.
(44) Akkerman, H. B.; de Boer, B. *J. Phys.: Condens. Matter* **2008**, 20.
(45) Patolsky, F.; Zheng, G.; Lieber, C. M. *Nat. Protocols* **2006**, *1*, 1711.
(46) Cui, Y.; Lieber, C. M. *Science* **2001**, *291*, 851.
(47) Fisher, W. R.; Taniuchi, H.; Anfinsen, C. B. *J. Biol. Chem.* **1973**, *248*, 3188.